4916 *Inorg. Chem.* **2010**, *49*, 4916–4921
DOI: 10.1021/ic902445c

Inorganic Chemistry
Article

Luminescence Dynamics in Tb^{3+}-Doped $CaWO_4$ and $CaMoO_4$ Crystals

Enrico Cavalli,*,† Philippe Boutinaud,‡ Rachid Mahiou,§ Marco Bettinelli,⊥ and Pieter Dorenbos∥

†*Dipartimento di Chimica Generale ed Inorganica, Chimica Analitica, Chimica Fisica, Università di Parma, Parma, Italy,* ‡*Laboratoire des Matériaux Inorganiques, Clermont Université, ENSCCF, BP10448, F-63000 Clermont-Ferrand, France,* §*CNRS, UMR6002, F-63177 Clermont-Ferrand, France,* ⊥*Laboratory of Solid State Chemistry, DB, Università di Verona, and INSTM, UdR Verona, Verona, Italy, and* ∥*Faculty of Applied Sciences, Delft University of Technology, Delft, The Netherlands*

Received December 9, 2009

Single crystals of $CaWO_4$ and $CaMoO_4$ doped with Tb^{3+} have been grown by the flux growth method. Their luminescence properties have been investigated in the 10−600 K temperature range under different experimental conditions. In spite of very similar spectra at low temperature upon excitation at 365 nm, the crystals show a very different behavior as the temperature is raised or the excitation wavelength is changed. These differences have been accounted for on the basis of models that take into consideration the position of the energy levels of the rare earth relative to the bandgap of the host material.

1. Introduction

There is an increasing interest in Tb^{3+}-doped tungstates and molybdates as new active media for phosphor technology.[1−3] In this perspective more effort is presently being devoted to the development of suitable synthetic strategies[4,5] than to the analysis of the processes governing the luminescence dynamics. Hence, the optimization of the phosphor performances is usually achieved by means of comparative tests that, even if effective from a practical viewpoint, do not always provide significant information on the luminescence dynamics. We think, however, that this aspect is important and deserves a thorough investigation.[6] The present paper is focused on $CaWO_4$:Tb^{3+} and $CaMoO_4$:Tb^{3+}, two materials already known for their interesting luminescence properties.[4,7,8] We have grown single crystals of $CaWO_4$ and $CaMoO_4$ doped with Tb^{3+} and measured their luminescence spectra and emission decay profiles in different experimental conditions at temperatures ranging from 10 to 600 K. The experimental results evidence significant differences in the spectroscopic behavior of the two compounds. The data have been analyzed in the framework of models accounting for the effects of the host lattice on the excited-state dynamics of rare earth dopants such as Pr^{3+} or Tb^{3+}.

2. Experimental Section

2.1. Crystal Growth and Properties. $CaWO_4$ (CWO) and $CaMoO_4$ (CMO) single crystals nominally doped with 0.5 mol % Tb^{3+} were grown by the flux growth method using Na_2WO_4 or Na_2MoO_4 as a solvent in the 1350−600 °C temperature range.[9] Analytical grade CaO (98%, Carlo Erba), Na_2CO_3 (99%, Aldrich), WO_3 (99%, Aldrich) or MoO_3 (99.5%, Aldrich), and Tb_4O_7 (99.9%, Aldrich) were used as starting materials. The crystals have a tetragonal scheelite ($CaWO_4$) structure with space group $I4_1/a$ and unit cell parameters a = 5.243 Å and c = 11.376 Å for CWO[10] and a = 5.226 Å and c = 11.430 Å for CMO.[11] The Tb^{3+} ions occupy the Ca^{2+} sites with 8-fold oxygen coordination (distorted dodecahedron, actual point group S_4). The difference in charge is compensated by the accommodation of Na^+ ions, present in the growth mixture, or by the formation of cationic vacancies. Whatever the case, it implies perturbations of the crystal field around the active ions and then some inhomogenous broadening of the spectral features. The electronic structures of the host matrices have been extensively investigated[12−15] and are still the subject of

*Corresponding author. E-mail: enrico.cavalli@unipr.it.

(1) Liao, J.; Qiu, B.; Wen, H.; You, W. *Opt. Mater.* **2009**, *31*, 1513–1516.
(2) Liao, J.; Qiu, B.; Wen, H.; Chen, J.; You, W. *Mater. Res. Bull.* **2009**, *4*, 1863–1866.
(3) Wang, Z.; Liang, H.; Wang, Q.; Luo, L.; Gong, M. *Mater. Sci. Eng., B* **2009**, *164*, 120–123.
(4) Li, G.; Wang, Z.; Quan, Z.; Li, C.; Lin, J. *Cryst. Growth Des.* **2007**, *7*, 1797–1802.
(5) Hou, Z.; Li, C.; Yang, J.; Lian, H.; Yang, P.; Chai, R.; Cheng, Z.; Lin, J. *J. Mater. Chem.* **2009**, *19*, 2737–2746.
(6) Cavalli, E.; Boutinaud, P.; Cucchietti, T.; Bettinelli, M. *Opt. Mater.* **2009**, *31*, 470–473.
(7) Van Uitert, L. G.; Soden, R. R. *J. Chem. Phys.* **1960**, *32*, 1161–1164.
(8) Zhang, Z.-J.; Chen, H.-H.; Yang, X.-X.; Zhao, J.-T. *Mater. Sci. Eng., B* **2007**, *145*, 34–40.
(9) Cavalli, E.; Bovero, E.; Belletti, A. *J. Phys. Condens. Matter* **2002**, *14*, 5221–5228.
(10) Zalkin, A.; Templeton, D. H. *J. Chem. Phys.* **1964**, *40*, 501–504.
(11) Gürmen, E.; Daniels, E.; King, J. S. *J. Chem. Phys.* **1971**, *55*, 1093–1097.
(12) Zhang, Y.; Holzwarth, N. A. W.; Williams, R. T. *Phys. Rev. B* **1998**, *57*, 12738–12750.
(13) Fujita, M.; Itoh, M.; Takagi, S.; Shimizu, T.; Fujita, N. *Phys. Status Solidi B* **2006**, *243*, 1898–1907.
(14) Groenink, J. A.; Hakfoort, C.; Blasse, G. *Phys. Status Solidi A* **1979**, *54*, 329–336.

Published on Web 05/13/2010

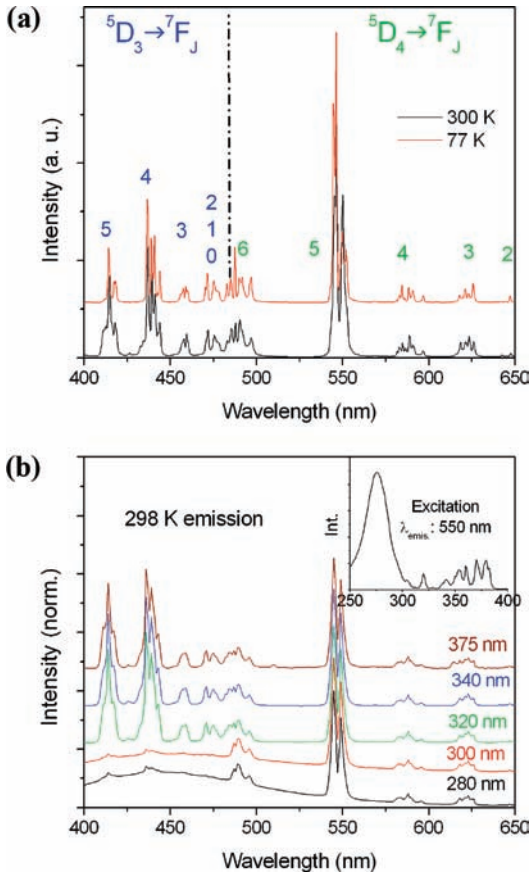

Figure 1. (a) 77 and 298 K emission spectra of $CaWO_4:Tb^{3+}$. $\lambda_{exc.}$: 360 nm. (b) Room-temperature emission of $CaWO_4:Tb^{3+}$ measured upon different excitation wavelengths. The excitation spectrum is shown in the inset.

discussion. On the basis of the most recent developments, we located the energy values of the fundamental excitation (FE) (corresponding to the lowest excitation peak) at 4.2. eV in the CMO and 5.2 in the CWO case, and those of the conduction bands at 4.5 and 5.6 eV, respectively.

2.2. Spectroscopic Measurements. The 10 K emission spectra were recorded using a spectroscopic system consisting of a 450 W Xe lamp fitted with a 0.22 Spex Minimate monochromator as source and a 1.26 m Spex monochromator with a RCA C31034 photomultiplier to analyze and detect the output radiation. The crystals were mounted onto the coldfinger of a He-cryocooler (Air Products Displex DE-202). The 300−600 K spectra were measured using a Triax 550 monochromator equipped with a nitrogen-cooled CCD camera and a R928 Hamamatsu photomultiplier (Jobin-Yvon Symphony system). The excitation light was selected from a xenon lamp using a Triax 180 monochromator. The samples were mounted on a homemade copper holder heated by a thermocoax wire connected to a Thermolyne regulator. The decay profiles were measured in the 10−300 K temperature range upon 355 nm laser excitation using a pulsed Nd:YAG laser (Quanta System model SYL 202); the emission was isolated by means of a Hilger−Watts model D330 double monochromator and detected with a Hamamatsu R943-022 photomultiplier connected to a LeCroy WS422 transient digitizer.

3. Emission Measurements

3.1. CWO:Tb^{3+}. The energy level composition and the low-temperature spectra of CWO:Tb^{3+} have already

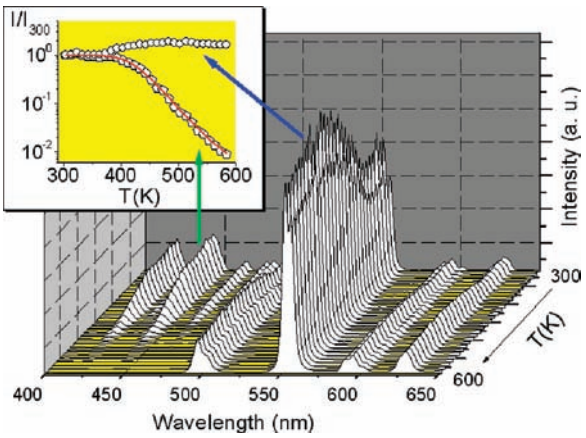

Figure 2. Emission spectra of $CaWO_4:Tb^{3+}$, measured in the 300−600 K temperature range. The temperature behaviors of the integrated intensities of the 440 and 550 nm bands are reported in the inset. The red line represents the fit by means of the Struck and Fonger model (eq 4) of the $^5D_3$ intensity profile.

been thoroughly investigated in the past.[16−18] The luminescence spectra measured at 77 and 300 K (Figure 1a) upon 360 nm excitation (in correspondence with the Tb^{3+} absorption) are in agreement with previous literature. They have similar intensity and are composed of both $^5D_3$ and $^5D_4$ emission features having, as expected, a significant broadness (full width at half-maximum, fwhm, on the order of 75−80 cm^{-1} at low temperature) as a consequence of the doping mechanisms. The wavelength dependence of the emission is shown in Figure 1b. It can be noted that excitation at wavelengths shorter than 320 nm (see the excitation spectrum reported in the inset of the figure) induces only a weak $^5D_3$ luminescence overlapping the broad tungstate emission and a more intense $^5D_4$ emission. The overlap integral between tungstate emission and Tb^{3+} absorption is nonzero for both $^5D_3$ (ground-state absorption at 382 nm) and $^5D_4$ (487 nm) states. The fact that the energy transfer process results in the preferential population of the $^5D_4$ level allows inferring that another mechanism is involved in the depletion of the $^5D_3$ level. In order to explore this aspect, we have measured the temperature evolution of the emission in the 300−600 K range upon excitation at 360 nm. The results, reported in Figure 2, show that the intensity of the $^5D_4$ emission slightly increases with the temperature, whereas that of the $^5D_3$ rapidly decreases above 400 K, as evidenced in the inset of the figure.

The decay profiles of both $^5D_3$ and $^5D_4$ emissions have been measured in the 10−298 K range upon 355 nm pulsed laser excitation. The $^5D_3$ curves are reported in Figure 3a. They can be reproduced by the Inokuti−Hirayama model for energy transfer in the absence of migration:[19]

$$\phi(t) = A \exp\left[-\frac{t}{\tau} - \alpha\left(\frac{t}{\tau}\right)^{3/s}\right] \quad (1)$$

(15) Treadway, M. J.; Powell, R. C. *J. Chem. Phys.* **1974**, *61*, 4003–4011.

(16) Wortman, D. E. *Phys. Rev.* **1968**, *175*, 488–498.
(17) Leavitt, R. P.; Morrison, C. A.; Wortman, D. E. *J. Chem. Phys.* **1974**, *61*, 1250–1251.
(18) Page, A. G.; Godbole, S. V.; Sastry, M. D. *J. Phys. Chem. Solids* **1989**, *50*, 571–575.
(19) Inokuti, M.; Hirayama, F. *J. Chem. Phys.* **1965**, *43*, 1978–1989.

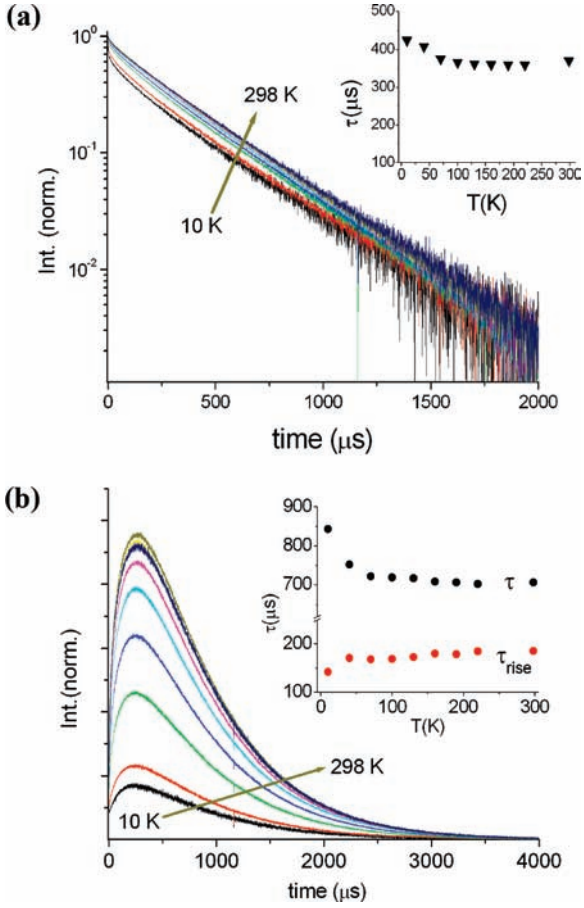

Figure 3. (a) Decay profiles of the $^5D_3$ emission of $CaWO_4:Tb^{3+}$, measured as a function of the temperature upon 355 nm excitation (emission wavelength: 410 nm). In the inset the temperature dependence of the decay times has been reported. (b) Decay profiles of the $^5D_4$ emission of $CaWO_4:Tb^{3+}$, measured as a function of the temperature upon 355 nm excitation (emission wavelength: 540 nm). In the inset the temperature dependence of both decay and rise times has been reported.

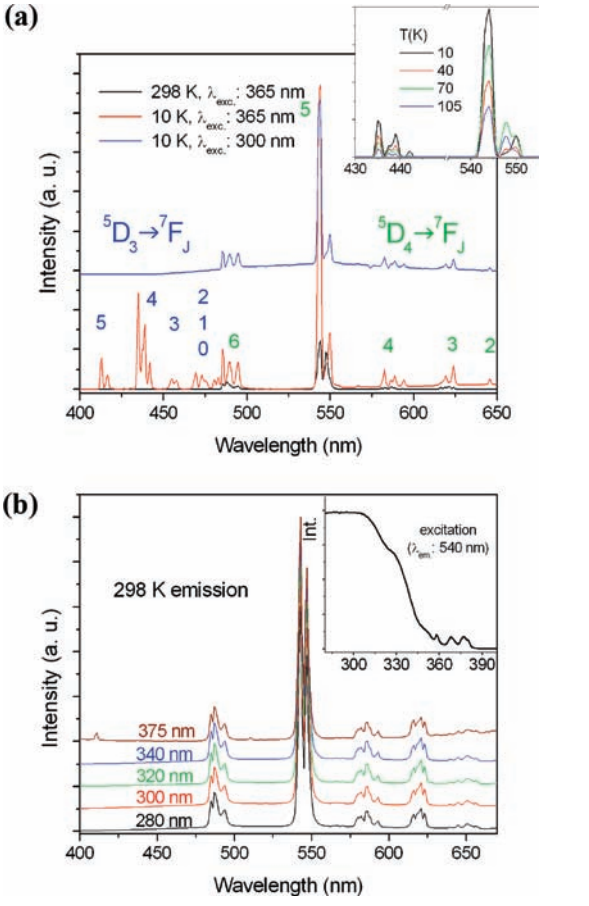

Figure 4. (a) Low-temperature emission spectra of $CaMoO_4:Tb^{3+}$. Inset: temperature evolution of the $^5D_3 \rightarrow {}^7F_4$ and $^5D_4 \rightarrow {}^7F_5$ manifolds in the 10−105 K range. (b) Room-temperature emission spectra of $CaMoO_4:Tb^{3+}$, measured upon different excitation wavelengths. Excitation spectrum is shown in the inset.

where $\phi(t)$ is the emission intensity after pulsed excitation, A is the intensity of the emission at $t = 0$, τ is the lifetime of the isolated donor, α is a parameter containing the energy transfer probability, and $s = 6$ for dipole−dipole (D-D), 8 for dipole−quadrupole (D-Q), and 10 for quadrupole−quadrupole (Q-Q) interaction. We have fitted the decay curves by means of eq 1 by considering a D-D process and A, τ, and α as adjustable parameters. The τ value obtained from the fit is 425 μs at 10 K and gradually decreases to 360−370 μs as the temperature increases up to 100 K; then it remains constant (see inset of Figure 3a). This small change can be tentatively accounted for by the variation of the thermal population of the Stark levels of the emitting $^5D_3$ state. The parameter α provides information on the probability of the energy transfer process:

$$\alpha = \frac{4}{3}\pi\Gamma\left(1-\frac{3}{s}\right)N_a R_0{}^3 \qquad (2)$$

where Γ is the gamma function, N_a the concentration of the acceptor expressed in ions·cm^{-3}, and R_0 is the critical distance. The value of α deduced from the 10 K decay profile is 0.85, and that of the critical distance is about 12 Å, compatible with the average distance between the active ions (15 Å) evaluated by considering a statistical distribution of the dopants inside the host lattice. This value is typical for cross-relaxation processes involving Tb^{3+} ions in solids.[20−22] The $^5D_4$ decay curves are shown in Figure 3b. They can be fitted to a difference of two exponentials, allowing the evaluation of both the rise time and the decay time of the emitting level. The rising component varies from 140 to 180 μs. These values are significantly shorter than the $^5D_3$ decay times of the isolated donor deduced from the Inokuti−Hirayama model. However they are consistent with the 1/e decay times calculated from the profiles of Figure 3a, indicating that feeding occurs from the $^5D_3$ state. The $^5D_4$ decay times range from 615 to 550 μs (see inset of Figure 3b), indicating that probably the $^5D_4$ emission is scarcely affected by nonradiative processes.

3.2. CMO:Tb^{3+}. We have summarized in Figure 4a the results of emission measurements in the 10−298 K range. The 10 K spectrum excited at 365 nm is very similar to the spectra of CWO:Tb^{3+} (see Figure 1) and can be commented on accordingly. Nevertheless, its temperature dependence is very different: a strong decrease of the luminescence intensity occurs in the 10−100 K range (see inset

(20) Park, J. Y.; Jung, H. C.; Rama Raju, G. S.; Moon, B. K.; Kim, J. H. *J. Lumin.* **2010**, *130*, 478–482.
(21) Bodenschatz, N.; Wannemacher, R.; Heber, J.; Mateika, D. *J. Lumin.* **1991**, *47*, 159–167.
(22) Tachihante, M.; Zambon, D.; Arbus, A.; Zahir, M.; Sadel, A.; Cousseins, J. C. *Mater. Res. Bull.* **1993**, *28*, 605–613.

of Figure 4a for some representative features), and at 300 K practically only the $^5D_4$ emission is present. This behavior cannot be ascribed to multiphonon relaxation (MPR) for at least two reasons: first because it has not been observed in the case discussed above despite the fact that calcium tungstate and molybdate have very similar vibrational properties[23] and, second, because the gap between the $^5D_3$ and the next lower lying $^5D_4$ level, on the order of 5500 cm^{-1}, requires more than six high-energy phonons (about 880 cm^{-1}) to be bridged. We therefore conclude on the existence of a host-related quenching channel for the $^5D_3$ emission in CMO:Tb^{3+}. In the 10 K spectrum measured upon excitation at 300 nm, i.e., in correspondence with the host absorption, the $^5D_4$ luminescence overlaps the orange broad band molybdate emission and no features originating from $^5D_3$ are present. Since there is no overlap between the host emission and the $^5D_3$ absorption band (at about 380 nm), we assume that the energy transfer from the host populates only the $^5D_4$ level. The room-temperature emission spectra measured for different excitation wavelengths are shown in Figure 4b. The $^5D_3$ luminescence is nearly absent, except for a very weak feature being present only in the 375 nm excited spectrum. For excitation wavelengths shorter than 375 nm a weak host emission is still observable. The excitation spectrum, shown in the inset of Figure 4b, presents the Tb^{3+} 4f-4f features (350−390 nm), the host-related broad band (below 320 nm) and a shoulder in the 330 nm region. The origin of this band will be discussed in the following. The measurements in the high-temperature regime (Figure 5) evidence a total thermal quenching of the $^5D_4$ emission in the 400−600 K range. The integrated intensity of the $^5D_4 \rightarrow {}^7F_5$ transition is reported in the inset of the figure as a function of the temperature.

The decay profiles of both $^5D_3$ and $^5D_4$ emissions have been measured as a function of the temperature. The $^5D_3$ curves are reported in Figure 6a. Up to 70 K these curves can be reproduced by means of eq 1 for a D-D process, yielding τ values in the 270−280 μs range. The value of the α parameter at 10 K is 1.32, and that of the critical distance obtained from eq 2 is about 14 Å, close to the average distance between the doping ions (15 Å) evaluated by statistical considerations. These values are consistent with those obtained for CWO:Tb^{3+}, indicating that in the low-temperature limit the emission dynamics of the two systems are similar and affected by the energy transfer process. As the temperature exceeds 70 K, the decays become faster and faster and the Inokuti−Hirayama fit becomes worse. The temperature dependence of the evaluated decay times is plotted in the inset of Figure 6a. The decay profiles of the $^5D_4$ luminescence are plotted in Figure 6b. In their long time tail they are always single exponential with decay times ranging from 460 to 520 μs, indicating that this emission is not significantly affected by nonradiative processes up to room temperature. The short time region shows a more complex behavior: up to 70 K the curves are nearly coincident and present a rising component with a time constant on the order of 70−75 μs. Increasing further the temperature

(23) Basiev, T. T.; Sobol, A. A.; Voronko, Y. K.; Zverev, P. G. *Opt. Mater.* **2000**, *15*, 205–216.

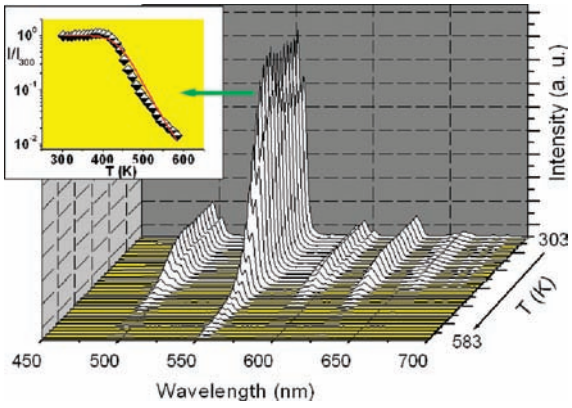

Figure 5. Emission spectra of $CaMoO_4$:Tb^{3+}, measured in the 300−600 K temperature range. The temperature behavior of the integrated intensity of the 540 nm band is reported in the inset. The red line represents the fit by means of the Struck and Fonger model (eq 4).

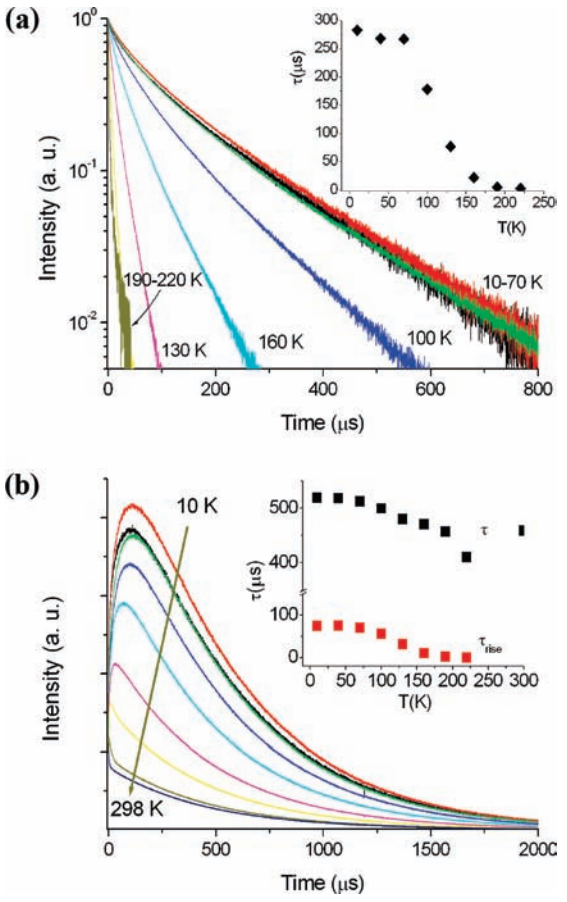

Figure 6. (a) Decay profiles of the $^5D_3$ emission of $CaMoO_4$:Tb^{3+}, measured as a function of the temperature upon 355 nm excitation (emission wavelength: 410 nm). In the inset the temperature dependence of the decay times is reported. (b) Decay profiles of the $^5D_4$ emission of $CaMoO_4$:Tb^{3+}, measured as a function of the temperature upon 355 nm excitation (emission wavelength: 540 nm). In the inset the temperature dependence of both decay and rise times is reported.

leads to a progressive shortening of the rise time, which falls to zero at about 200 K. This allows the observation of a short-lived component ascribed to the molybdate emission (the 355 nm excitation being in correspondence with a residual host absorption). This component is certainly present also in the low-temperature curves and affects their initial profiles. This accounts for the discrepancy

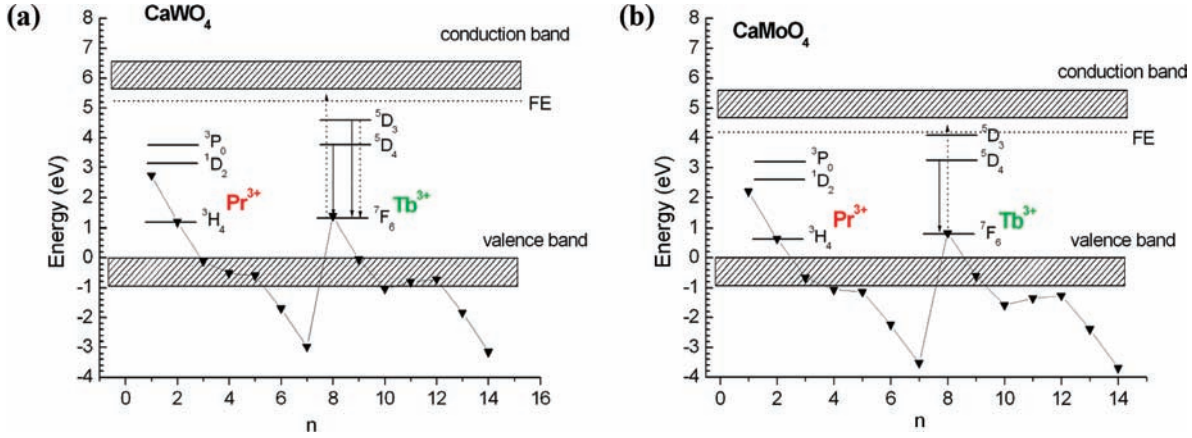

Figure 7. Position of the ground-state energy along the Ln^{3+} series in $CaWO_4$ (a) and $CaMoO_4$ (b).

observed between the low-temperature values of the rise time and of the $^5D_3$ decay time. In contrast to the case of CWO:Tb^{3+}, the particular temperature dependence of the decay curves of CMO:Tb^{3+} in the short time range clearly demonstrates a change in the relaxation mechanism of the $^5D_3$ level between 70 and 200 K. This point will be discussed in the next section.

3. Discussion

CWO:Tb^{3+} and CMO:Tb^{3+} crystals exhibit very similar emission spectra at low temperature, upon Tb^{3+} excitation. This indicates that the coordination symmetries and then the crystal fields (CF) around the active ions are nearly identical, as expected on the basis of their structural properties. However, the spectra measured upon host excitation as well as the temperature behavior of both emitted intensities and decay profiles are strongly host dependent and cannot be accounted for by considering only the properties of the isolated centers. In the past 10 years Dorenbos has been collecting data and models specifically aimed at constructing and predicting the location of lanthanide impurity electronic levels relative to those of the host compound; see, for example, ref 24. The parameter set required to construct level schemes is still occasionally being refined and improved.[25] The most recent parameter set can be found in ref 26, where also schemes are reported on the relative position of the energy levels of the rare earth trivalent (and divalent) ions with respect to the bandgap of a number of host lattices. We think that this could be a suitable starting model in order to interpret the emission properties of the Tb^{3+}-doped crystal. This scheme can be compiled on the basis of the following considerations. In the presence of oxidizing ions such as d^0 closed-shell transition metals (M^{n+} = Ti^{4+}, V^{5+}, Nb^{5+}, Ta^{5+}, Mo^{6+}, W^{6+}) it is possible to observe the photoinduced redox process

$$Tb^{3+} + M^{n+} \rightarrow Tb^{4+} + M^{(n-1)+}$$

concomitant with the formation of an intervalence charge transfer (IVCT) state that actively participates in the fluorescence dynamics of the system. This process usually gives rise to a band in the excitation spectrum.[27] In the investigated materials however, the assignment of the IVCT bands is not a simple task, since the excitation spectra of the host emissions are complicated by the presence of features ascribed to defective centers.[14,15] It is, however, possible to estimate with good approximation the energy of an IVCT transition by means of the empirical equation proposed by Boutinaud et al.:[28]

$$\mathrm{IVCT}(Ln^{3+}, cm^{-1}) = 58\,800 - 49\,800\left(\frac{\chi_{opt}(M^{n+})}{d_{min}(Ln^{3+} - M^{n+})}\right) \quad (3)$$

where $\chi_{opt}(M^{n+})$ is the optical electronegativity of the d^0 transition metal ion and $d_{min}(Ln^{3+}-M^{n+})$ its shortest distance from the lanthanide (Pr^{3+} or Tb^{3+}) ion. The calculated values, about 330 nm for CMO and 310 nm for CWO, are in correspondence with shoulders observed on the low-energy side of the experimental excitation bands (insets of Figures 1b and 4b) and can be considered reasonable. The IVCT can be considered an electronic transition from the ground state of the rare earth to the transition metal constituting the lattice,[29] and its energy provides information on the location of the Tb^{3+} levels relative to the host bands. The method to construct level schemes proposed by Dorenbos[26] allows then extending this information to all trivalent lanthanide ions. The obtained schemes, shown in Figure 7 for the ground-state energies (with the exception of Pr^{3+} and Tb^{3+}, for which also the excited levels are shown), are of general utility. The procedure applied to construct these schemes is extensively described in ref 26. Here E_{FE} is referred to as the energy of the fundamental excitation, i.e., the maximum of the host excitation band. We proposed in ref 26 that the bottom of the conduction band (CB) is located at about 1.08 times E_{FE} above the top of the valence band (VB) and that the energy of the electron after IVCT is at 1.04 times E_{FE} above the top of the VB. All energy levels represented in the schemes should be viewed as electron-donating levels. The energy on the vertical axis is then the difference between the energy required to remove an electron from the level involved and the energy necessary to remove an electron from the top of the valence

(24) Dorenbos, P. *J. Phys.: Condens. Matter* **2000**, *15*, 8417–8434.
(25) Dorenbos, P. *J. Alloys Compd.* **2009**, *488*, 568–573.
(26) Dorenbos, P.; Krumpel, A. H.; van der Kolk, E.; Boutinaud, P.; Bettinelli, M.; Cavalli, E. *Opt. Mater.*, doi:10.1016/j.optmat.2010.02.021.
(27) Boutinaud, P.; Putaj, P.; Mahiou, R.; Cavalli, E.; Speghini, A.; Bettinelli, M. *Spectrosc. Lett.* **2007**, *40*, 209–220.
(28) Boutinaud, P.; Cavalli, E.; Bettinelli, M. *J. Phys.: Condens. Matter*, **2007**, *19*, 386230 (1−11).
(29) Krumpel, A.; van der Kolk, E.; Dorenbos, P.; Boutinaud, P.; Cavalli, E.; Bettinelli, M. *Mater. Sci. Eng., B* **2008**, *147*, 114–120.

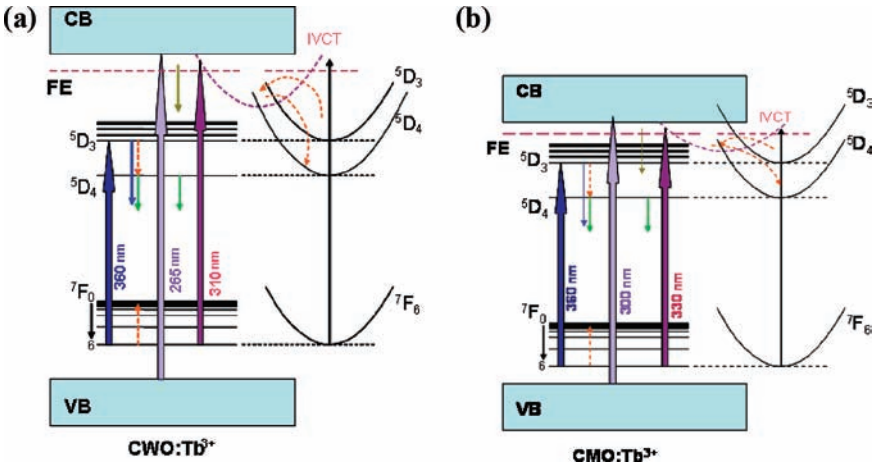

Figure 8. Energy level scheme and fluorescence dynamics in $CaWO_4$:Tb^{3+} (a) and $CaMoO_4$:Tb^{3+} (b). The solid lines represent the absorption (excitation) and radiative emission processes; the dotted lines describe the nonradiative processes.

band. The two models can be improved on the basis of the present experimental results relative to the Tb^{3+} ion. The temperature behavior of the $^5D_3$ emission of CWO:Tb^{3+} (Figure 2) can be analyzed by means of the Struck and Fonger model[30] for a thermally induced crossover to a Franck−Condon shifted state:

$$\frac{I(T)}{I_0} = \left[1 + A\left(\frac{E}{kT}\right)\right]^{-1} \quad (4)$$

where A is close to 10^7 and E is the activation energy from the $4f^n$ state to its crossover with the quenching state (here the IVCT one). The fit of the profile reported in the inset of Figure 2 provides a value of about 5500 cm^{-1} for the activation energy. This energy has been used to compile the diagram shown in Figure 8a. This scheme allows understanding the excitation wavelength dependence of the emission reported in Figure 1b: excitation in the 300−250 nm range results in fact in the population of the IVCT state that preferentially relaxes to the $^5D_4$, almost bypassing the $^5D_3$ state. In the case of CMO:Tb^{3+} there is no high-temperature $^5D_3$ emission, whereas the temperature dependence of the $^5D_4$ level emission in the 400−600 K range is reasonably reproduced using eq 4, yielding a value of about 5700 cm^{-1} for the activation energy. On this basis we have compiled the scheme of Figure 8b, which allows understanding the temperature behavior observed in Figure 5. The relative position of the $^5D_3$ and IVCT potential curves is in fact compatible with thermalization occurring even at low temperature, resulting in the concomitant $^5D_3$ depopulation and $^5D_4$ population through the IVCT state.

Let us now take into consideration the decay curve measurements. The $^5D_3$ and $^5D_4$ decay profiles of CWO: Tb^{3+} evidence an energy transfer process in which the $^5D_3$ level decays nonradiatively to $^5D_4$. In agreement with previous literature,[31] we conclude that this process consists of the cross-relaxation mechanism:

$$^5D_3, {}^7F_0 \rightarrow {}^5D_4, {}^7F_6$$

represented by means of dotted arrows in Figure 8a. The weak temperature dependence of the resulting decay times accounts for the nearly (but not completely) resonant character of the process, the involved energy gaps being about 5800 cm^{-1} ($^5D_3$−$^5D_4$) and 5750 cm^{-1} ($^7F_0$−$^7F_6$), as reported for Tb^{3+} in LaF_3.[32] By considering the thermal behavior of the $^5D_3$ emission, which is practically constant up to 400 K (see inset of Figure 2), we can conclude that in the 150−400 K temperature range this temperature-independent quenching channel is prevalent, at the present dopant concentration, upon other quenching processes occurring through the IVCT level. For CMO:Tb^{3+} the situation is rather different: in the low-temperature regime the energy transfer process takes place as in the previous case. For temperatures above 70−80 K, however, the shapes of both $^5D_3$ and $^5D_4$ profiles change significantly, and this behavior cannot be accounted for by invoking phonon-mediated effects. According to Figure 8b, we are in the presence of a progressive change in the $^5D_3$ depleting mechanism involving the thermal population of the IVCT state and its radiationless decay by crossover to the $^5D_4$ level. This mechanism is consistent with the progressive shortening of the $^5D_3$ decay times and of the related rise times in the emission profile of $^5D_4$. In this case the crossover to the IVCT state appears to be more important than cross-relaxation processes.

4. Conclusions

The optical spectra of $CaWO_4$ and $CaMoO_4$ crystals doped with Tb^{3+}, measured in different experimental conditions, evidence significant differences that cannot be ascribed to the isolated centers. The observed phenomena have been accounted for in the framework of a unitary model that involves the formation of an IVCT state participating in the excited-state dynamics of the systems. This has implied the compilation of a "host lattice plus rare earth dopant" energy level scheme that has been demonstrated to be effective in the analysis of the experimental observations. This approach will be soon extended to other systems in order to confirm its validity.

Acknowledgment. The Italian authors acknowledge the MIUR (Italian Ministry for the University and the Scientific Research) for the financial support in the course of the project PRIN 2007.

(30) Struck, C. W.; Fonger, W. H. *J. Appl. Phys.* **1971**, *42*, 4515–4516.
(31) May, P. S.; Sommer, K. D. *J. Phys. Chem. A* **1997**, *101*, 9571–9577.
(32) Carnall, W. T.; Crosswhite, H.; Crosswhite, H. M. *Energy level structure and transition probabilities of the trivalent lanthanides in LaF_3*; Argonne National Laboratories: Argonne, IL, 1977.